Integrated mechanical and material design of quasi-zero-stiffness vibration isolator with superelastic Cu-Al-Mn shape memory alloy bars

Yoshikazu Araki[1*], Kosuke Kimura[1], Takehiko Asai[2], Takeshi Masui[3], Toshihiro Omori[4], Ryosuke Kainuma[4]

1. Department of Architecture and Architectural Engineering, Kyoto University, Katsura, Nishikyo, Kyoto 615-8540, Japan.
2. Disaster Prevention Research Institute, Kyoto University, Gokasho, Uji 611-0011, Japan
3. Department of Architecture, Kansai University, Yamate, Suita 564-8680, Japan
4. Department of Materials Science, Tohoku University, Aoba, Sendai 980-8579, Japan

Corresponding author

*Yoshikazu Araki, e-mail: araki@archi.kyoto-u.ac.jp, +81-75-383-2924

Keywords

Quasi-zero-stiffness (QZS), Vertical vibration isolation, Earthquake ground motion, Shape memory alloy (SMA), Superelasticity, Cu-Al-Mn alloy, Shaking table test

Abstract

Quasi-zero-stiffness (QZS) vibration isolators avoid excessive deformation due to gravity, a critical issue in *vertical* vibration isolation, by providing restoring force with high initial stiffness and low tangent stiffness around the static equilibrium position. Effective use of geometric nonlinearity often plays a central role in QZS mechanisms. Design of such QZS mechanisms, however, tends to be complex, and it is difficult to realize large loading capacity as well as large stroke length at the same time. This paper attempts to resolve these issues by applying newly developed superelastic Cu-Al-Mn shape memory alloy (SMA) bars, characterized by excellent recoverable strain upon unloading along with small hysteresis and nearly flat stress plateau. These features are realized by material design tailored for obtaining mechanical properties required in QZS mechanisms. The use of such tailored superelastic Cu-Al-Mn SMA bars allows us to easily achieve large loading capacity as well as large stroke length while keeping the QZS mechanism simple and compact. In this paper, we derive design equations, produce a prototype, and conduct shaking table tests and numerical simulations to demonstrate the feasibility of QZS vibration isolator with superelastic Cu-Al-Mn SMA bars.

1. Introduction

In the design of vertical vibration isolators, excessive deformation due to gravity force is one of the main obstacles. To overcome the difficulty, many papers have been published on quasi-zero-stiffness (QZS) vibration isolators [1,2]. In QZS vibration isolators, the problem of excessive deformation due to gravity force is overcome by providing restoring force with the following two characteristics: (1) the initial stiffness is high in the small displacement range, and (2) the tangent stiffness is low in the operating range around the static equilibrium position when subjected to gravity force. The term of QZS comes from the second characteristic of the low tangent stiffness. Such vibration isolators are also referred to as high-static-low-dynamic-stiffness (HSLDS) vibration isolators [3].

In the literature, geometric nonlinearity, or the nonlinear relationship between the restoring force and the change of geometric configurations, is often used to realize the QZS property [1-3]. In these types of QZS vibration isolators, a combination of linear springs and/or post-buckled beams are typically used. Another type of QZS vibration isolators presented in the literature use magnets [4,5]. While a large stroke length of tens to hundreds millimeter is required in some applications like seismic isolation, the stroke length of the QZS isolators presented in the literature is limited to less than ten millimeter. In order to realize a stroke length large enough for seismic isolation, the mechanical design of QZS mechanisms tends to be complex and involved. This is especially true when large loading capacity is also required.

Araki et al. [6,7] proposed simple QZS mechanisms having a large stroke length by applying constant-force springs, which sustain constant load regardless of their elongation. The loading capacity of a single constant-force spring is, however, limited to the order of tens to hundreds newton while the size of a constant-force spring is relatively large. To achieve large loading capacity in QZS mechanisms, e.g., several to tens kilonewton, a number of constant-force springs become necessary, which makes the size of QZS mechanisms unnecessarily large. This limits the range of applicability of QZS vibration isolators with constant-force springs to light weight applications.

To resolve this issue, this paper studies the use of superelastic shape memory alloys (SMAs) in QZS vibration isolators. In general, shape recovery of SMAs is caused by either heating or unloading [8,9]. Shape recovery caused by heating is called *shape memory effect*, and that by unloading is called *superelastic effect* or *superelasticity*. The SMAs with superelasticity are referred to as *superelastic SMA*s. Superelastic SMAs are suitable for passive vibration isolation, and a bunch of literature exists on the use of superelastic SMAs in *horizontal* vibration isolation [8,9]. On the other hand, the literature on the use of superelastic SMAs in *vertical* vibration isolation is scarce. To the authors' knowledge, the only exception is the pioneering work by Lagoudas et al. [10]. The stroke length of their QZS vibration isolator is, however, also less than ten millimeter. It appears difficult to increase both the stroke length and the loading capacity because SMAs are used in the form of tube springs. Furthermore, the hysteresis of Ni-Ti superelastic SMAs is relatively large while such large hysteresis degrades the vibration isolation capability in vertical vibration isolation [6,7].

In order to realize QZS mechanism having large loading capacity and stroke length along with small hysteresis, this paper explores the feasibility of the use of newly developed superelastic Cu-Al-Mn SMA bars, characterized by the material design tailored for obtaining excellent recoverable strain along with small hysteresis and nearly flat stress plateau. To obtain excellent recoverable strain, grains much larger than bar diameter are developed by repeating heat treatment [11]. Furthermore, grain orientation is controlled by cold drawing and annealing to achieve small hysteresis and nearly flat stress plateau, which are the key features of the superelastic Cu-Al-Mn SMA bars used in this paper. Moreover, compared to most popular Ni-Ti SMAs, Cu-Al-Mn SMAs are superior in material cost, machinability, and loading rate dependence [12-14]. In the present QZS mechanism, elongation of horizontally placed superelastic Cu-Al-Mn SMA bars is converted into vertical motion of the vibration isolator. This mechanism is an extension from the QZS mechanism developed by Araki et al. [7]. The replacement of constant-force springs with superelastic SMA bars is the main difference in the extension. The replacement along with the tailored material design of superelastic Cu-Al-Mn SMA bars enables us to easily increase the loading capacity by a factor of tens to hundreds while keeping the size and the stroke length of the QZS mechanism. Or, conversely, the size of the QZS mechanism can be decreased by a factor of tens to hundreds while keeping the loading capacity and the stroke length. Along with the simplicity of the QZS mechanism, these are the new and key features of the QZS vibration isolator presented in this paper.

In this paper, first, we present design equations for the present QZS mechanism. Second, a prototype of the QZS vibration isolator with a superelastic Cu-Al-Mn SMA bar is designed and produced. In the prototype design, we seek the possibility of reducing the size of the QZS mechanism without changing the loading capacity from the QZS vibration isolator with constant-force springs tested in reference [7]. Shaking table tests and numerical simulations are finally conducted to assess the performance of the present QZS vibration isolator.

2. Design equations

Figure 1 schematically illustrates the present QZS mechanism. A superelastic SMA bar is placed horizontally at the center height of the vibration isolator as shown in Figure 1(a). With this configuration, superelastic SMA bar is subject to only tension force, which minimizes the use of SMA bar. The motion of both ends of the SMA bar is constrained by the upper and lower trapezoidal plates. Each end of the SMA bar is connected to a roller shaft, indicated by a white circle in Figure 1(a). Roller bearings are used to realize frictionless contact between the roller shafts and the upper and lower plates. The shapes of the plates are both symmetric with respect to the central vertical axis. Both plates have the same size and are placed symmetrically with respect to the central horizontal axis. Define by θ the angle between the vertical axis and the side edge of the trapezoid. As shown in Figure 1(b), let u denote the relative displacement between the upper and lower plates whose positive direction is shrinkage. Let f be the restoring force of the vibration isolator which is positive when the vibration isolator is subject to compression. Let e and n be the elongation and tensile axial force of the SMA bar, respectively.

Figure 2(a) shows the free body diagram of the upper plate, where r is the internal force. From this free body diagram, the equilibrium equation in the vertical direction can be written as

$$f = 2r\sin\theta\ . \tag{1}$$

Figure 2(b) shows the free body diagram of the right end of the SMA bar and the right roller shaft. From this diagram, the equilibrium equation in the horizontal direction can be written as

$$n = 2r\cos\theta\,. \tag{2}$$

From equations (1) and (2), the relationship between f and n can be written as

$$\frac{f}{n} = \tan\theta\,. \tag{3}$$

Figure 2(c) depicts the relationship between u and e. The gray objects (lines and circles) indicate the initial configuration while the black ones indicate the deformed configuration. The circles depict the right roller shaft, and the solid lines indicate the right lower corner of the upper plate. From Figure 2(c), the relationship between u and e can be written as

$$\frac{u}{e} = \frac{1}{\tan\theta}\,. \tag{4}$$

Let k_T be the tangent stiffness of the vibration isolator and d_T be the tangent stiffness of the SMA bar. Noting that equations (3) and (4) hold for infinitesimal changes of f, u, n, and e, denoted by $\mathrm{d}(\ )$, we can write the relationship between k_T and d_T as

$$k_\mathrm{T} = \frac{\mathrm{d}f}{\mathrm{d}u} = \left(\tan\theta\right)^2 \frac{\mathrm{d}n}{\mathrm{d}e} = \left(\tan\theta\right)^2 d_\mathrm{T}\,. \tag{5}$$

Figure 3(a) illustrates a restoring force curve model of the vibration isolator. This figure also illustrates the shift of axes to consider the vibration around the static equilibrium position. The dotted line shows a hypothetical restoring force curve when no hysteresis exists. Here, m is the mass of the object to be isolated, g is the gravitational acceleration, h indicates the hysteresis amplitude in f originated from the hysteresis of superelastic SMA bars, and u_S, u_L, u_U indicate the displacements relative to the base at the static equilibrium position, the lower bound, and the upper bound, respectively. The lower and upper bounds are determined so that the stroke of the vibration isolator covers the range wherein k_T has a constant value around the static equilibrium position. Define the shifted restoring force Δf and the shifted relative displacement Δu by

$$\Delta f = f - m\mathrm{g}\,,\ \Delta u = u - u_\mathrm{S}\,. \tag{6}$$

As shown in Figure 3(b), the range of Δu is limited by the upper bound $\Delta u_\mathrm{U} = u_\mathrm{U} - u_\mathrm{S}$ and the lower bound $\Delta u_\mathrm{L} = u_\mathrm{L} - u_\mathrm{S}$. Suppose that the vibration isolator is subject to the base acceleration $\ddot{u}_\mathrm{B}$. Then the equation of motion in the vertical direction for the vibration isolator can be written as

$$m\left(\Delta\ddot{u} + \ddot{u}_\mathrm{B}\right) + c\Delta\dot{u} + k_\mathrm{T}\Delta u + q = 0\,, \tag{7}$$

where c is the damping coefficient and over dot indicates differentiation with respect to time t. Here, q is the friction force inherent in the vibration isolator, which can be obtained only from the quasi-static tests of the whole vibration isolator. Assume that the friction force can be expressed as Coulomb's friction, where b is the amplitude of q, i.e., q changes between $-b$ and b depending on the sign of $\Delta\dot{u}$ as

$$q = \begin{cases} b & \text{if } \Delta\dot{u} > 0 \\ 0 & \text{if } \Delta\dot{u} = 0 \\ -b & \text{if } \Delta\dot{u} < 0 \end{cases}. \tag{8}$$

Also assume that the vibration isolator is designed so that the damping force $c\Delta\dot{u}$ is negligibly small. Then, this is a well-known bilinear hysteretic oscillator and its properties, e.g., transmissibility, free vibration response, and seismic response, have been extensively studied by many researchers [15-17]. This paper estimates the upper bound of the response acceleration by using the following simple design equation to assess the combined effects of lowered natural frequency and force limiting nature of hysteresis. Define ω_T by $\omega_\mathrm{T} = \sqrt{k_\mathrm{T} / m}$. Then, dividing equation (7) by m , we obtain

$$\Delta\ddot{u} + \ddot{u}_\mathrm{B} + \frac{c}{m}\Delta\dot{u} + \omega_\mathrm{T}^2 \Delta u + \frac{q}{m} = 0 \ . \tag{9}$$

Let Δu_P be the peak (maximum absolute) value of Δu . From equation (9), the absolute response acceleration $\left|\Delta\ddot{u} + \ddot{u}_\mathrm{B}\right|$ can be bounded as

$$\left|\Delta\ddot{u} + \ddot{u}_\mathrm{B}\right| \le \frac{h+b}{m} + \omega_\mathrm{T}^2 \Delta u_\mathrm{P} \ , \tag{10}$$

where the first and second terms of the right-hand side of equation (10) express the effects of the hysteresis and the natural frequency, respectively. It can be seen from equation (10) that reducing the hysteresis as well as the natural frequency is important for achieving excellent vibration isolation capability.

3. Prototype design

Compared to the QZS mechanism using constant-force springs [6,7], the use of superelastic Cu-Al-Mn SMA bars enables us to easily increase the loading capacity by a factor of tens to hundreds while keeping the size and the stroke length of the QZS mechanism. Or, conversely, the size of the QZS mechanism can be decreased by a factor of tens to hundreds while keeping the loading capacity and the stroke length. In the prototype design in this paper, we seek the possibility of decreasing the size of the QZS mechanism.

The dimensions of the superelastic Cu-Al-Mn SMA bar used in the present vibration isolator are shown in Figure 4. The length of the bar is 300 mm with 30 mm threading on both ends. The diameter is 11 mm in the threaded portions and 7 mm in the remaining center portion. In order to obtain excellent recoverable strain, grains much larger than bar diameter, called bamboo grains, are developed by repeating heat treatment [11]. Furthermore, to obtain nearly flat stress plateau and small hysteresis with little dependence on strain amplitude, grain orientations of the Cu-Al-Mn SMA bar in the drawing direction are controlled to be <1 1 0> in the bamboo structure, whose estimated recoverable strain is around 8% [12], by cold drawing and annealing. The superelastic Cu-Al-Mn SMA bar is prepared by Furukawa Techno Material Co., Japan. The nominal composition is Cu-17.3 at.% Al-11.4 at.% Mn. The values of Martensite start temperature M_{s}, Martensite finish temperature M_{f}, Austenite start temperature A_{s}, and Austenite finish temperature A_{f} are $M_{\mathrm{s}} = -45.8$, $M_{\mathrm{f}} = -71.6$, $A_{\mathrm{s}} = -47.9$, and $A_{\mathrm{f}} = -23.9\,°\mathrm{C}$.

The gray line in Figure 5 depicts the restoring force curve obtained from the quasi-static tensile test conducted on the SMA bar. The tensile test was performed using a hydraulic testing machine with the target strain of 4% (9.36mm) and the strain rate of 3mm/min. As shown by the black line in Figure 5, design parameters are extracted from the tensile test based on a piecewise-linear approximation. The tangent stiffness in the operating range d_{T} is 217N/mm, and the restoring force at 6mm elongation (center of operating range) is 7.55kN.

Figure 6 shows the photograph of the present vibration isolator. The height of the vibration isolator at the static equilibrium position is 393mm. The stroke length of the vibration isolator is ±115mm. Figure 7 illustrates the plan and elevations of the vibration isolator, respectively. As shown in Figure 7(a), the QZS mechanism is located at the center of the vibration isolator and pantograph mechanisms are located at the outer portions in the *Y* direction. The pantograph mechanisms are installed to avoid rocking and horizontal motions of the upper table. As shown in these figures, a superelastic Cu-Al-Mn SMA bar, indicated by a black solid line, is placed horizontally in the *X* direction at the center of the QZS mechanism. As shown in Figure 8, each end of the SMA bar is connected to a roller shaft having 4 roller bearings. In Figures 7(a) and 7(c), roller bearings are indicated by transparent gray rectangles. The inner roller bearings are in contact with the inclined sides of the upper trapezoidal plates, while the outer roller bearings are in contact with the lower trapezoidal plates. The lower trapezoidal plates are fixed to the base plate, while the upper trapezoidal plates are fixed to the upper table, on which the object to be isolated is placed. With such a composition, the horizontal axial force n of the SMA bar is converted into the vertical restoring force f of the vibration isolator. Elongation e of the SMA bar is also amplified into the vertical relative motion of the vibration isolator u.

In the design of the prototype of the presented vibration isolator, the elongation of the SMA bar at the static equilibrium position is assumed to be 6mm (2.47% strain), and the range of elongation during vibration is assumed to be ±5mm (±2.14% strain). Note here that the maximum strain of 4.61% in the design is much less than the recoverable strain 8% estimated for the grain orientation of the present SMA bar. To achieve a stroke length over ±100mm for the vibration isolator, the angle θ of the trapezoids' sides is designed to satisfy $\tan\theta = 1/20$. The stroke length along with the loading capacity can be adjusted by changing the value of only one parameter θ, if necessary. Due to this characteristic, the adjustment can be performed easily while keeping the size of the vibration isolator compact. The adjustment becomes much easier and quicker if the upper and lower trapezoidal plates are replaced with the load conversion mechanism presented in reference [7].

It is worth noting that the size of the space necessary for installing superelastic SMA bar is about 1/100 or less compared to that for installing constant-force springs to achieve the same loading capacity in the QZS mechanism.

4. Experiments

Quasi-static and shaking table tests are performed to assess the vibration reduction performance of the present vibration isolator.

In the quasi-static tests, forced displacement is applied to the upper table manually with the loading rate slow enough, while the base plate is fixed to the ground. The displacement u of the upper table is obtained by non-contact laser displacement sensors. The restoring force f is obtained by the load cells installed between the ground and the base plate of the vibration isolator.

Figure 9(a) shows the restoring force curve obtained from the quasi-static test, and Figure 9(b) shows a numerical model calibrated to the test result. At the center of the range of movement of the vibration isolator, i.e., when the height of the upper table is 393mm, the restoring force is 338.5N and the tangent stiffness k_T is 0.55N/mm. It should be remarked that the experimentally obtained value of the tangent stiffness k_T is in good agreement with the design value of k_T =0.54N/mm obtained by substituting the experimentally observed value of d_T into equation (5). The sum of the amplified hysteretic force h of the SMA bar and the friction force b inherent in the vibration isolator, i.e. $h+b$, is 46.0N. From equation (10), the upper bound of the absolute response acceleration can be estimated as 0.136, 0.185, 0.234, and 0.282g for the maximum displacement of 0, 30, 60, and 90mm, respectively.

Shaking table tests are performed to investigate the vibration reduction performance of the presented vibration isolator. Figure 10 schematically illustrates the configuration of the experimental setup. The total mass *m* of the isolated object, the upper plate, and the pantograph mechanism is 34.5kg, Acceleration sensors are installed on the upper table of the vibration isolator to measure the response acceleration $\Delta\ddot{u}+\ddot{u}_\mathrm{B}$, and on the shaking table to record the input acceleration $\ddot{u}_\mathrm{B}$ at the base of the vibration isolator. Non-contact laser displacement sensors are fixed to a measurement frame placed on the ground to measure the response absolute displacement $\Delta u+u_\mathrm{B}$ and the input absolute displacement u_B. Response relative displacement Δu is obtained by subtracting u_B from $\Delta u+u_\mathrm{B}$. Sampling rate is 100Hz in both acceleration and displacement measurements.

Two types of base accelerations are applied as input waves. One input wave is the up-down (UD) component of the ground motion recorded at K-NET Ojiya station in Japan during the 2004 Mid Niigata Prefecture earthquake. Note here that the input wave is amplified so that the peak accelerations is 1.0g while the peak acceleration is 0.83g in the original record of K-NET Ojiya UD ground motion. The other input wave is a sinusoidal wave whose frequency and amplitude are 5Hz and 1.0g, respectively. It should be noted here that the value of the input frequency of 5Hz was selected in accordance with the loading capacity of the shaking table, where the input frequency should be larger than 3.9Hz in order to realize the input acceleration amplitude of 1.0g.

Figures 11 and 12 show the records of the time histories of the input acceleration $\ddot{u}_{\mathrm{B}}$, the response acceleration $\Delta\ddot{u}+\ddot{u}_{\mathrm{B}}$, and the response relative displacement Δu. Table 1 reports the peak values of $\ddot{u}_{\mathrm{B}}$, $\Delta\ddot{u}+\ddot{u}_{\mathrm{B}}$, and Δu. As can be observed from Figures 11 and 12 and Table 1, the peak response acceleration is reduced to about 0.2g, which is usually sufficient for seismic isolation. The upper bound values $|\Delta\ddot{u}+\ddot{u}_{\mathrm{B}}|$ of response acceleration, predicted by substituting the observed peak value of Δu into equation (10), are 0.18g and 0.16g for the earthquake and sinusoidal input waves, respectively. These values are fairly in good agreement with the recorded values shown in Table 1 while a slight discrepancy (0.06g) is observed between the design prediction (0.16g) and the experimental observation (0.22g) in the case of the sinusoidal input wave. This discrepancy is caused by high frequency vibrations induced possibly by backlash and friction in the bearings.

5. Simulations

In this section, we obtain transmissibility to examine the vibration isolation performance of the present vibration isolator in the frequency domain. For this purpose, numerical simulations are performed to obtain stationary response to sinusoidal base accelerations. The reasons for obtaining transmissibility by numerical simulations (not by experiments) are as follows. In the present vibration isolator, transmissibility inherently depends on the input amplitude because its restoring force is nonlinear [10]. Since the present vibration isolator is designed so that relatively large base accelerations (about 1.0g) are reduced to about 0.2g, which is a usual criterion in seismic isolation, the input acceleration amplitude used in the shaking table tests should be much larger than 0.2g. Furthermore, since the present vibration isolator is designed so that its resonant frequency is less than 1Hz, which is usual for seismic isolation purpose, low frequency input waves should be applied to identify the resonant frequency. In realizing such a large amplitude and low frequency input acceleration, the displacement amplitude of the input wave becomes very large (more than 1m). Note again that, as stated in Section 4, 3.9Hz is the lower bound of the input frequency for the shaking table used in the tests when the input acceleration amplitude of 1.0g is required. Also the amplitude of the response displacement of the vibration isolator at the resonant frequency can be very large (more than 1m), which is far beyond the stroke length of the present vibration isolator. For these reasons, it is very difficult, if not impossible, to obtain the transmissibility of the present vibration isolator from the shaking table tests.

In the numerical simulations, the Runge-Kutta method is used for time integration. The parameters are determined as m=34.5kg, c=0.03Ns/mm, k_T=0.54N/mm, $h+b$=46.0N. Here, the values of m, k_T , and $h+b$, are determined from the results of the quasi-static tests. On the other hand, the value of c is determined so that the damping ratio defined by $c/(2\sqrt{mk_{\mathrm{T}}})$ is 10%. This relatively large value of the damping coefficient is selected to examine the effect of neglecting the damping force in deriving equation (10) for estimating the peak response acceleration.

Figure 13 shows the transmissibility of the present vibration isolator to the input acceleration amplitudes of 0.5g and 1.0g obtained by the numerical simulations and by the theoretical predictions using equation (10). For comparison, Figure 13(b) also shows the experimentally obtained transmissibility for the input sinusoidal wave whose acceleration frequency and amplitude are 5Hz and 1.0g, respectively. From Figure 13, good agreement can be observed among the simulation results, theoretical predictions, and the experimental results. From Figure 13, it can also be seen that the resonant frequency is around 0.6Hz, which is much less than that of the vibration isolator with Ni-Ti SMA tube springs reported in reference [10].

6. Conclusions

A QZS vibration isolator with a superelastic Cu-Al-Mn SMA bar has been presented. The tailored material design of superelastic Cu-Al-Mn SMA bars and their application to QZS vibration isolator allow us to increase the loading capacity or to decrease the size of the QZS mechanism by a factor of tens to hundreds while keeping the stroke length large enough. Since the superelastic SMA takes care of the nonlinear properties necessary for QZS mechanism, the QZS mechanism itself and its design are both simple. These are the new and key features of the QZS vibration isolator presented in this paper. The feasibility of the present QZS vibration isolator has been demonstrated through shaking table tests, where input seismic and sinusoidal waves with the maximum accelerations of 1.0g were reduced to about 0.2g, which is in good agreement with the design equations derived in this paper. The transmissibility of the present vibration isolator, obtained by numerical simulations, has demonstrated that the resonant frequency of the present vibration isolator was about 0.6Hz and that the estimation error of the design equations was small enough.

Acknowledgement

This research was supported by the Toray Science Foundation. Mr. Nobutoshi Yoshida, a technical researcher of Kyoto University, and Mr. Yoshito Nojiri, a former undergraduate student of Kyoto University helped to conduct the experiments. The authors gratefully acknowledge the supports mentioned above.

References

[1] P. Alabuzhev, A. Gritchin, L. Kim, G. Migirenko, V. Chon, P. Stepanov, *Vibration Protecting and Measuring Systems with Quasi-Zero Stiffness*, Hemisphere Publishing, NY, 1989.

[2] R. Ibrahim, Recent advances in nonlinear passive vibration isolators, *Journal of Sound and Vibration*, 314 (3-5) (2008) 371–452.

[3] A. Carrella, *Passive vibration isolation with high-static-low-dynamic-stiffness*, Ph.D. thesis, University of Southampton, 2008

[4] A. Carrella A, M.J. Brennan, T.P. Waters, K. Shin, On the design of a high-static–low-dynamic stiffness isolator using linear mechanical springs and magnets, *Journal of Sound and Vibration*, 315 (3) (2008) 712–720.

[5] W.S. Robertson, M.R.F. Kidner, B.S. Cazzolato, Theoretical design parameters for a quasi-zero stiffness magnetic spring for vibration isolation, *Journal of Sound and Vibration*, 326 (1-2) (2009) 88–103.

[6] Y. Araki, T. Asai, T. Masui, Vertical vibration isolator having piecewise-constant restoring force, *Earthquake Engineering and Structural Dynamics*, 38 (13) (2009) 1505-1523.

[7] Y. Araki, T. Asai, K. Kimura, K. Maezawa, T. Masui, Nonlinear vibration isolator with adjustable restoring force, *Journal of Sound and Vibration*, 332 (23) (2013) 6063–6077.

[8] L. Lecce, A. Concilio, *Shape Memory Alloy Engineering for Aerospace, Structural and Biomedical Applications,* Elsevier Amsterdam, 2015.

[9] O.E. Ozbulut, S. Hurlebaus, R. Desroches, Seismic control using shape memory alloys: a review, *Journal of Intelligent Material Systems and Structure*, 22 (14) (2011)1531-1549.

[10] D.C. Lagoudas, M.M. Khan J.J. Mayes, B.K. Henderson, Pseudoelastic SMA spring elements for passive vibration isolation: Part II – Simulations and experimental correlations, *Journal of Intelligent Material Systems and Structures,* 15 (6) (2004) 443-470

[11] T. Omori, T. Kusama, S. Kawata, I. Ohnuma, Y. Sutou, Y. Araki, K. Ishida, R. Kainuma, Abnormal grain growth induced by cyclic heat treatment, *Science*, 341 (6153) (2013) 1500-1502.

[12] Y. Sutou, T. Omori, K. Yamauchi, N. Ono, R. Kainuma, K. Ishida, Effect of grain size and texture on pseudoelasticity in Cu–Al–Mn-based shape memory wire. *Acta Materialia* , 53 (15) (2005) 4121–4133.

[13] Araki Y, Endo T, Omori T, Sutou Y, Koetaka Y, Kainuma R, Ishida K (2011) Potential of superelastic Cu-Al-Mn alloy bars for seismic applications, *Earthquake Engineering and Structural Dynamics*, 40(1): 107-115.

[14] B. Gencturk, Y. Araki, T. Kusama, T. Omori, R. Kainuma, F. Medina, Loading rate and temperature dependency of Cu-Al-Mn superelastic alloy bars, *Construction and Building Materials*, 53 (2014) 555-560.

[15] R. Tanabashi, Studies on nonlinear vibration of structures subjected to destructive earthquakes, *Proceedings of the World Conference on Earthquake Engineering,*

Proceedings, Berkeley, California, 6-1–6-7, 1956.

[16] R. Pratap, S. Mukherjee, F.C. Moon, Dynamic behavior of a bilinear hysteretic elato-plastic oscillator, part I: free oscillations, *Journal of Sound and Vibration*, 172 (3) (1994) 321-337.

[17] N. Challamel, G. Gilles, Stability and dynamics of a harmonically excited elastic-perfectly plastic oscillator, *Journal of Sound and Vibration*, 301 (3-5) (2007) 608-634.

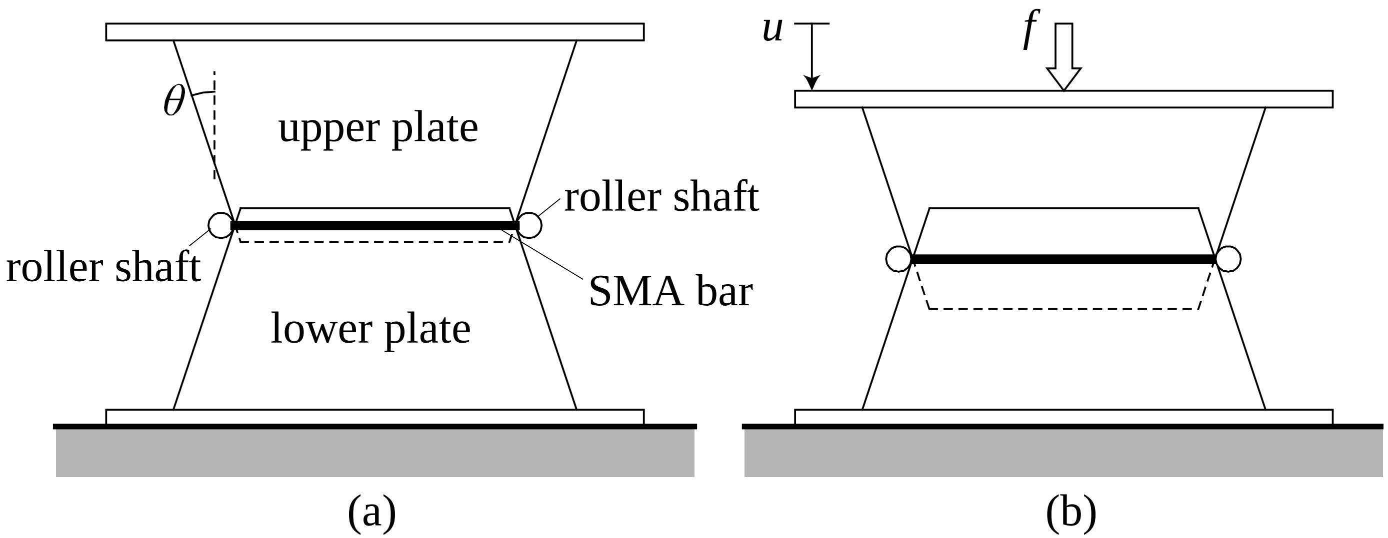

Figure 1. Schematic illustration of the motion conversion mechanism: (a) initial (undeformed) configuration and (b) deformed configuration.

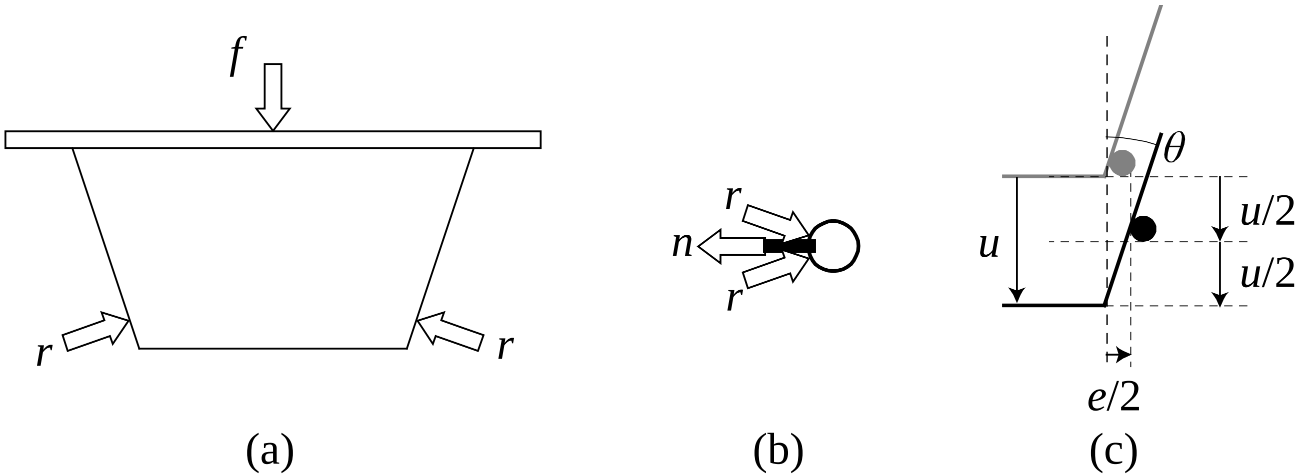

Figure 2. (a) Free body diagram of the upper plate. (b) Free body diagram of the right end of the SMA bar and the right roller shaft. (c) Geometric relationship between u and e at the right roller shaft.

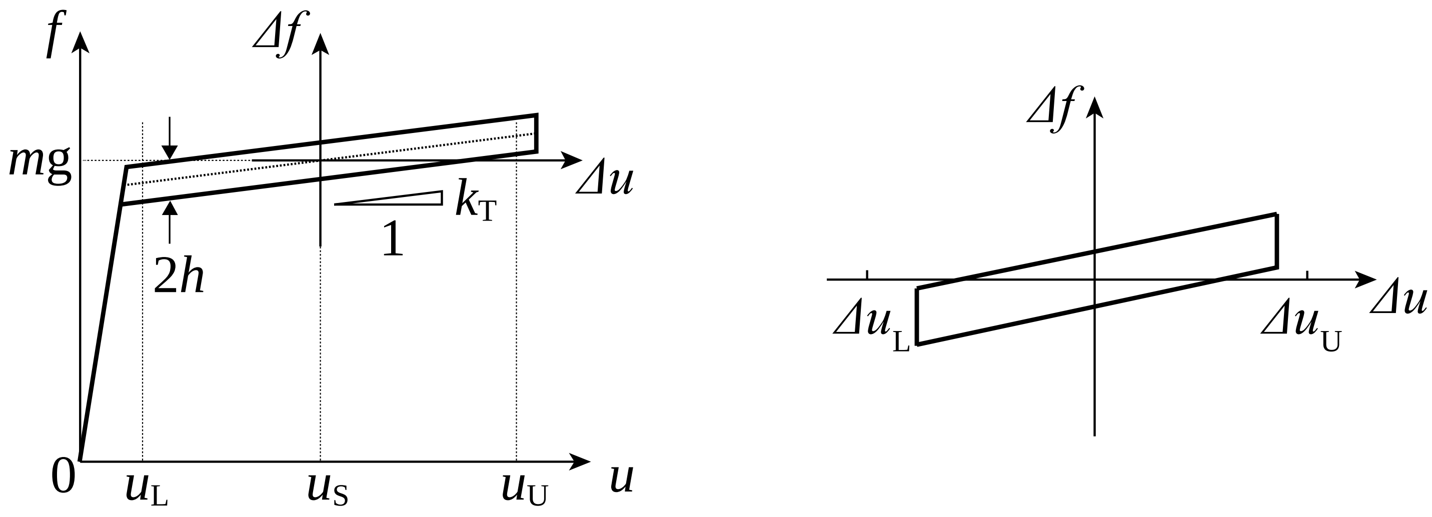

(a) (b)

Figure 3. (a) Relationship between the vertical relative displacement and the vertical restoring force provided by superelastic SMA bar. (b) The stroke of the vertical relative displacement around the static equilibrium position.

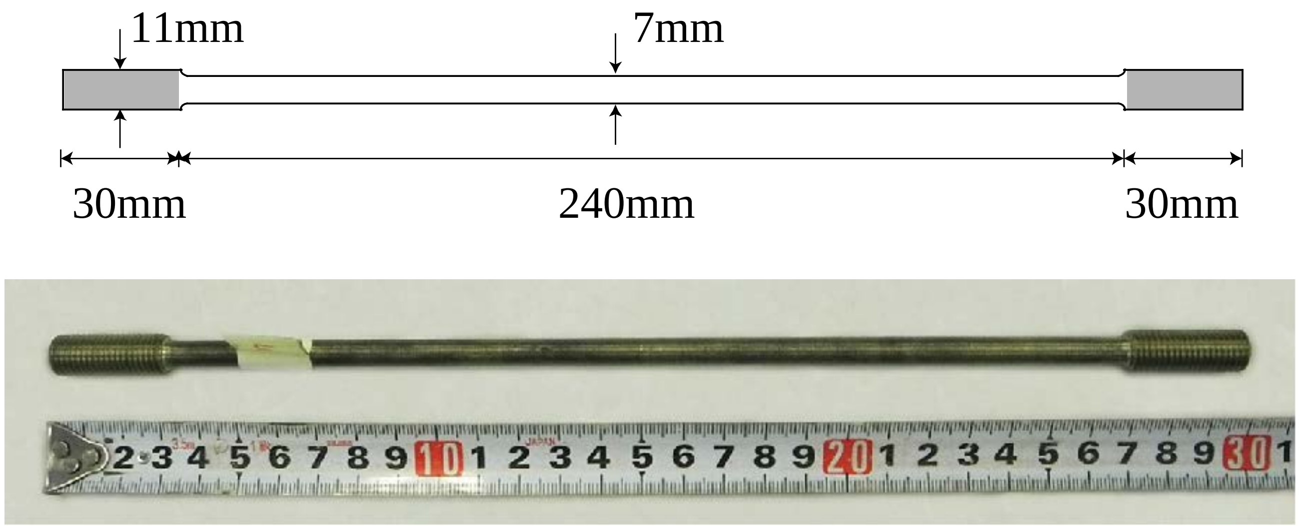

Figure 4. Size of the superelastic Cu-Al-Mn SMA bar.

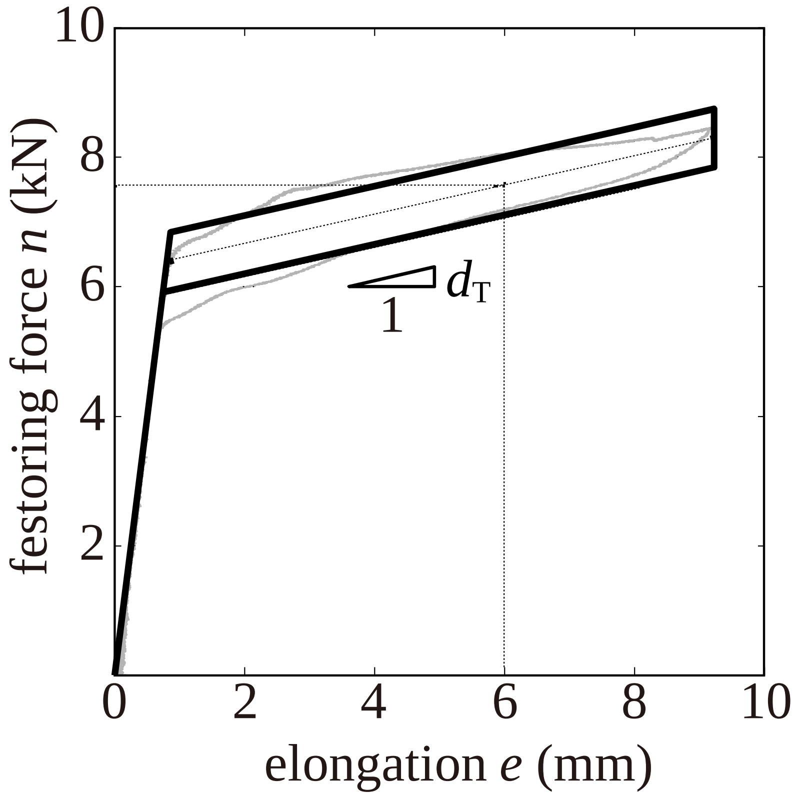

Figure 5. Restoring force curve of superelastic Cu-Al-Mn SMA bar

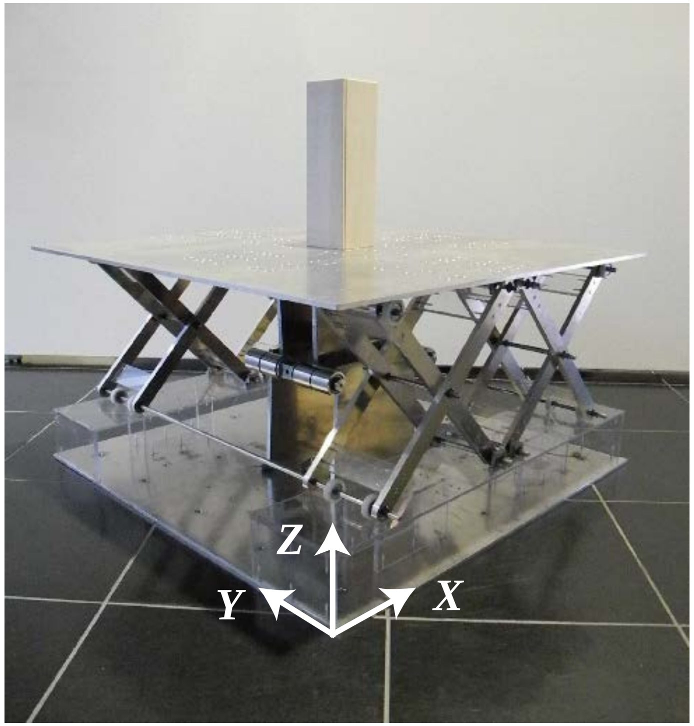

Figure 6. Photograph of the prototype of the vibration isolator.

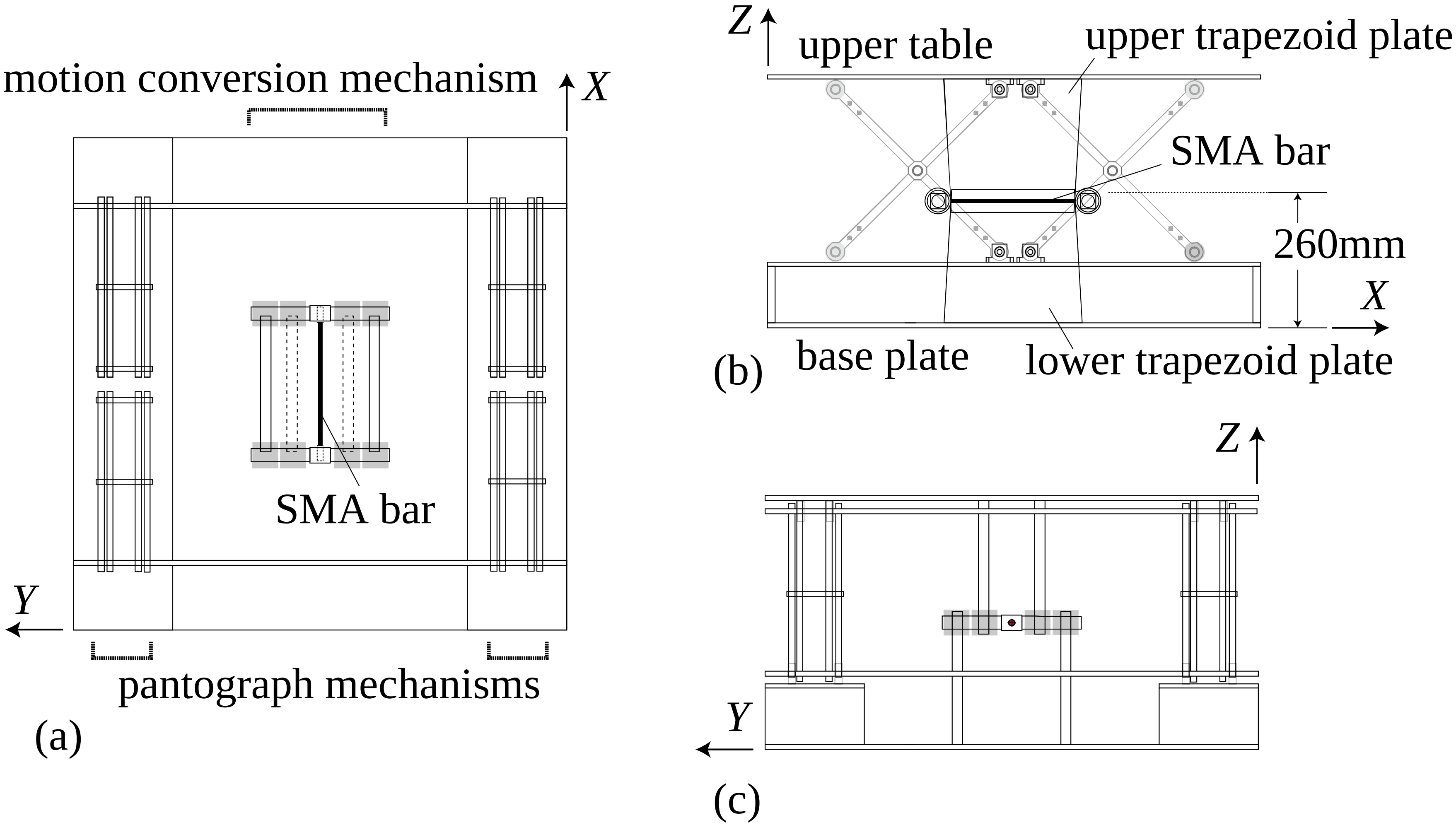

Figure 7. Prototype of the vibration isolator: (a) *X*-*Y* plan, (b) *Z*-*X* plane, and (b) *Y*-*Z* plane.

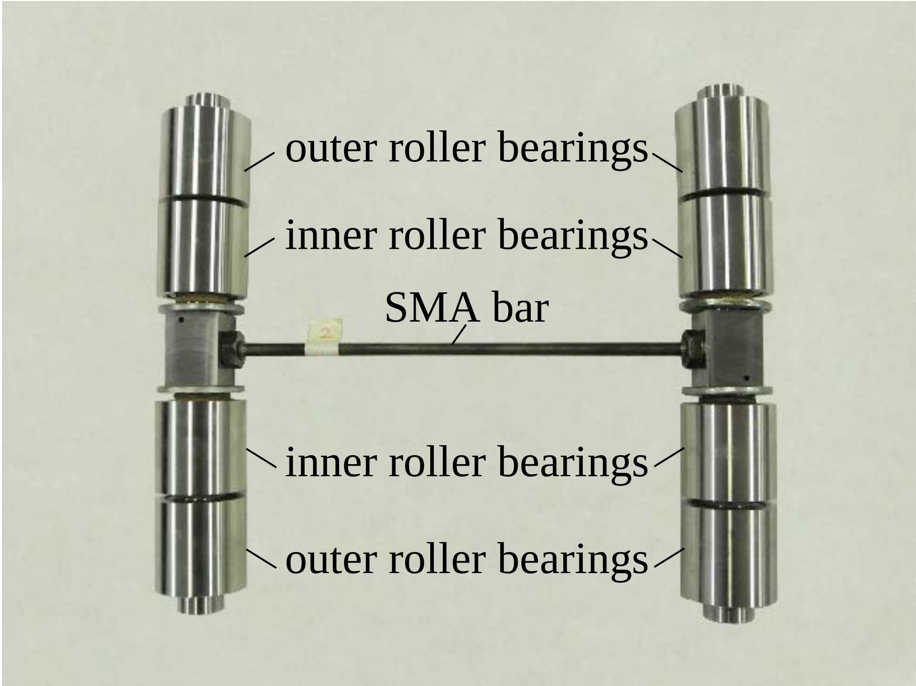

Figure 8. Photgraph of the SMA bar, the roller shafts, and the roller bearings.

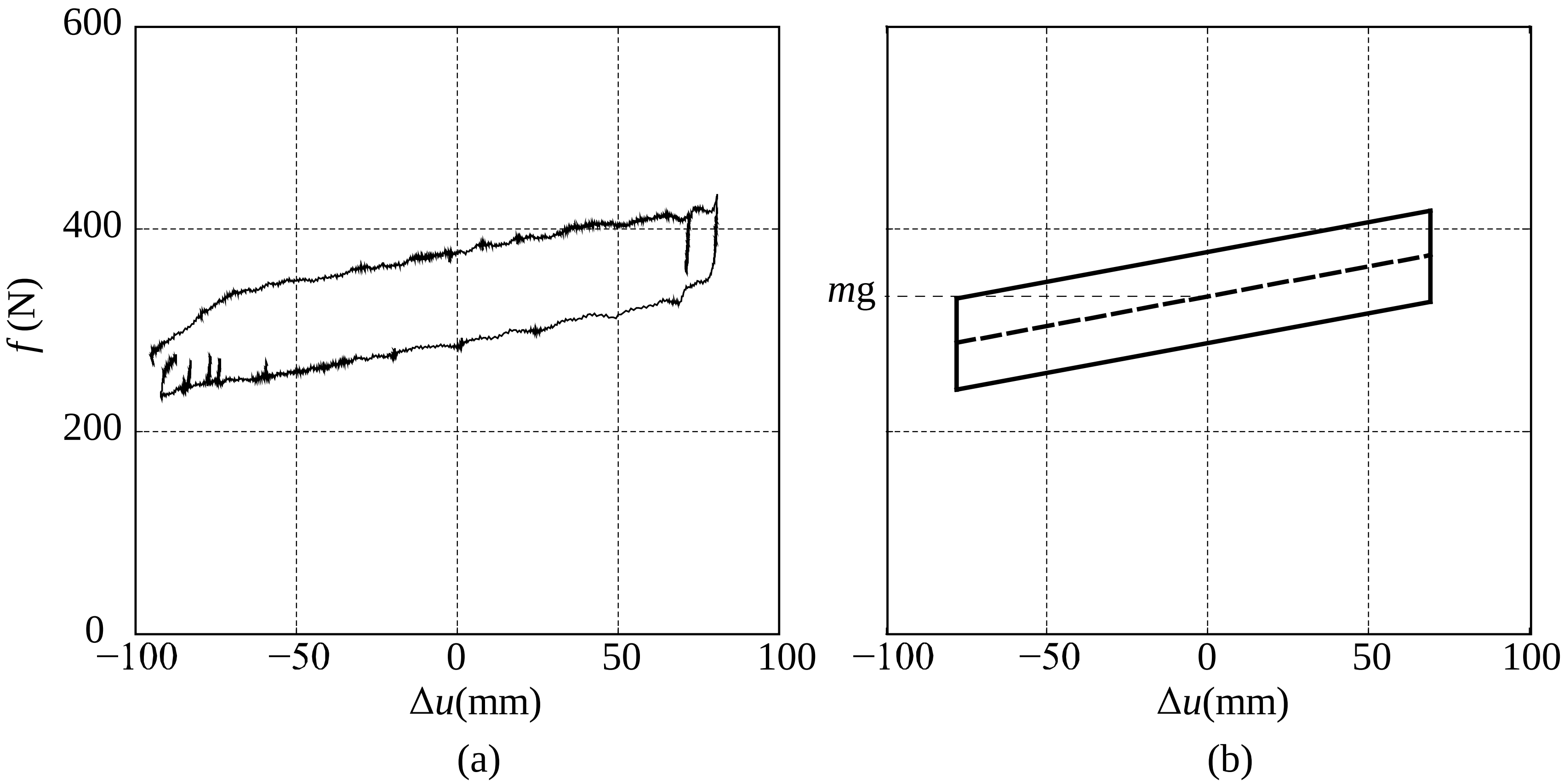

Figure 9. Restoring force curve: (a) quasi-static loading test result and (b) numerical model.

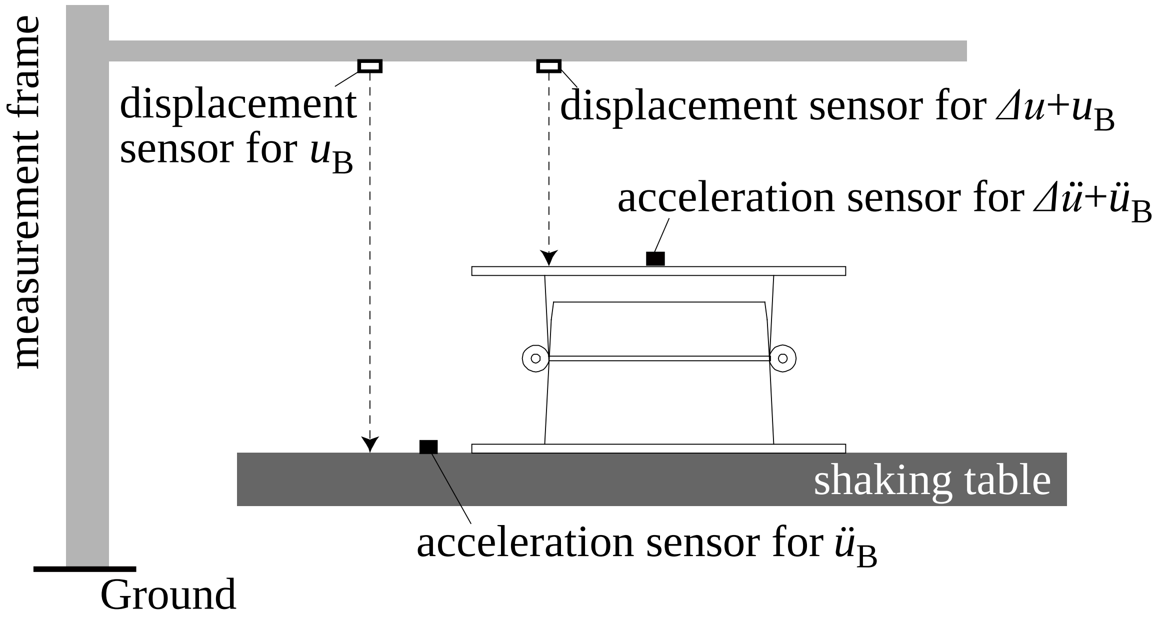

Figure 10. Schematic illustration of the setup for the shaking table tests.

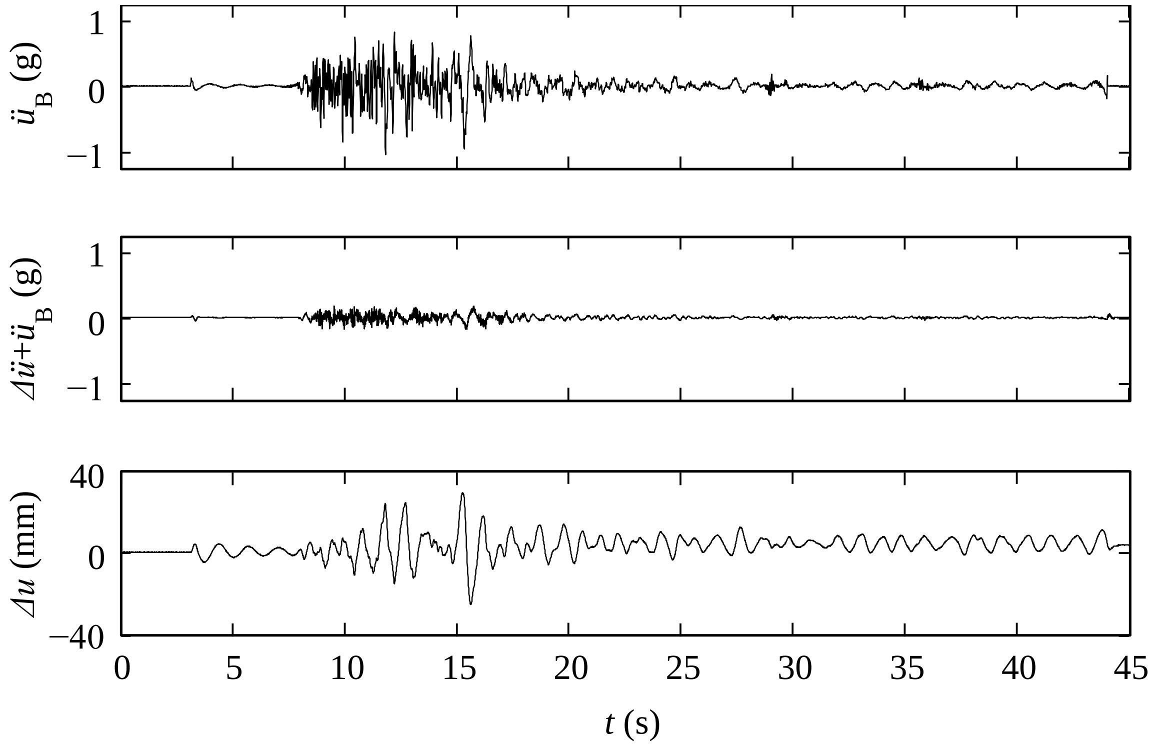

Figure 11. Time history records of input and response waves for K-Net Ojiya UD.

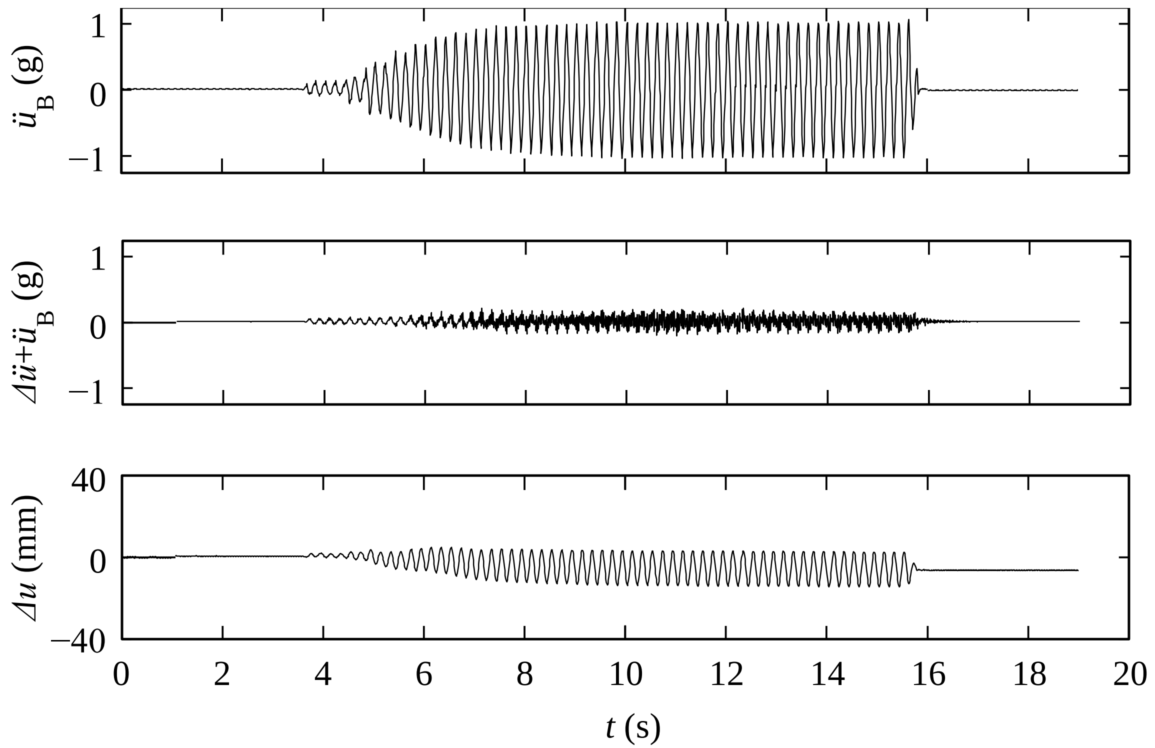

Figure 12. Time history records of input and response waves for sinusoidal 5Hz wave.

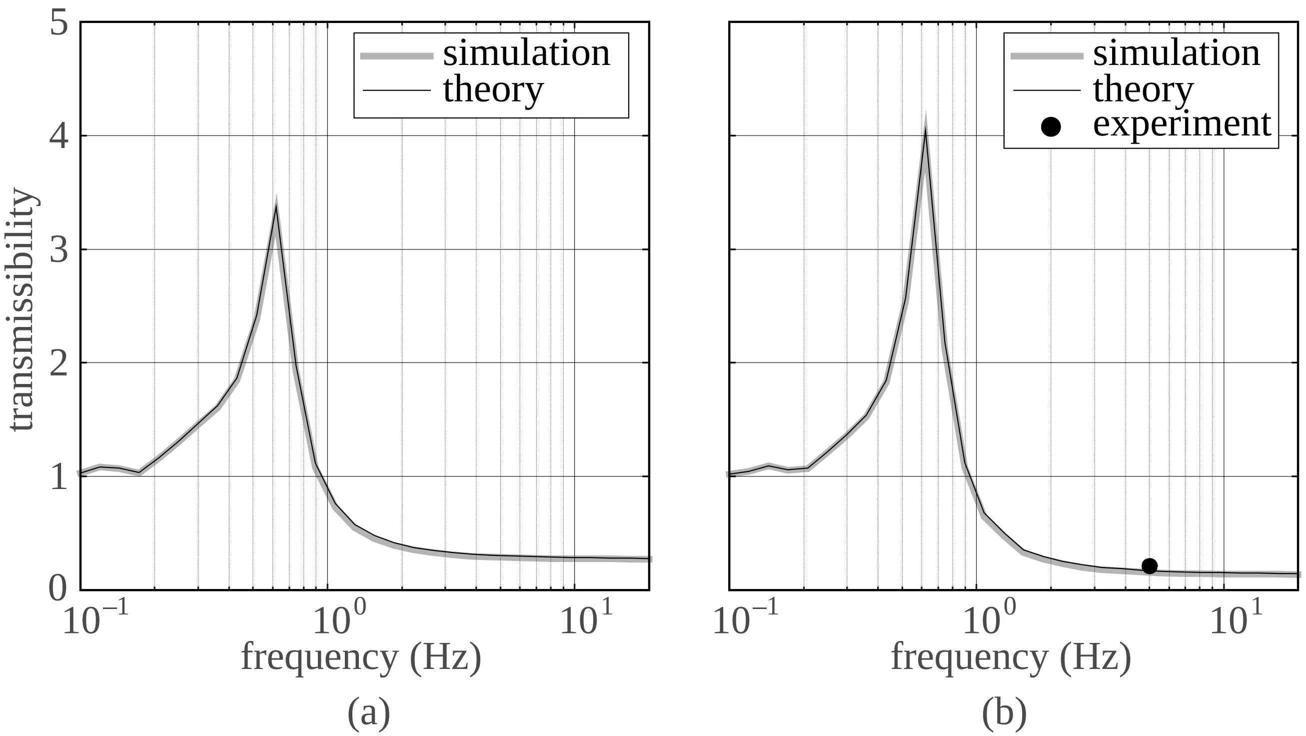

Figure 13. Transmissibility of the vibration isolator: (a) input amplitude=0.5g, (b) input ampitude=1.0g.

Table 1. Recorded peak values of input and response waves.

input wave	$\ddot{u}_{\mathrm{B}}$ (g)	$\Delta\ddot{u}+\ddot{u}_{\mathrm{B}}$ (g)	Δu (mm)
K-Net Ojiya UD	1.05	0.18	28.88
Sinusoidal 5Hz	1.06	0.22	14.98